2-D and 3-D Whole-Core Transport Calculations of the OECD Benchmark Problem C5G7 MOX by CRX

Nam Zin Cho, Gil Soo Lee, and Chang Je Park
Korea Advanced Institute of Science and Technology
Department of Nuclear and Quantum Engineering
373-1 Kusong-dong, Yusong-gu
Taejon, Korea 305-701
Email : nzcho@mail.kaist.ac.kr

ABSTRACT

2-D and 3-D heterogeneous transport calculations of OECD benchmark problem C5G7 MOX were performed with the CRX code and their results are given in this paper. For 3-D calculations, we use a fusion technique of 2D/1D methods: the method of characteristics (MOC) for radial 2-D calculation and the diamond difference (DD) scheme for axial 1-D calculation. To reduce computer memory and computation time, parallel processing and coarse mesh rebalance (CMR) acceleration are used.

1. INTRODUCTION

The CRX code based on the method of characteristics (MOC) has been constructed to treat 2-D whole-core heterogeneous calculation with features of modular ray tracing and parallel computing.[1][2][3]

Recently, a 2D/1D fusion method [4] was implemented in the CRX code for 3-D calculation. The 2D/1D fusion method, devised for 3-D problems, is a synergistic combination of the method of characteristics for radial 2-D calculation and the S_N-like method for axial 1-D calculation. Each solver sends and receives surface angular fluxes and thus requires some iterations. However, this new approach requires much less memory and takes advantage of the simpler structure of a core in axial direction, resulting in overall efficiency.

In this paper, we presents some results of the C5G7 MOX benchmark problem released by OECD/NEA [5] ; 2-D calculations with the original CRX code and 3-D calculations with the 2D/1D fusion method implemented in the CRX code.

2. DESCRIPTION OF THE 2-D CALCULATION

To treat large-scale complex problems, the CRX code uses modular ray tracing and direct ray sweeping. There are several parameters which determine accuracy of the calculation. In this paper, we solved the 2-D C5G7 MOX benchmark problem with various azimuthal angles (4-16) per octant and several choices of computational meshes (24-48) per cell. The standard calculation was performed with 8 azimuthal/ 2 polar angles per octant, 50 rays per cell and direction, and 40 computational meshes per cell.
To reduce computational time and memory, we used CMR/CGR acceleration and the parallel computation with angular decomposition, of which details have been reported in Refs. 2 and 3.

3. DESCRIPTION OF THE 3-D CALCULATION

For 3-D calculation, the 2D/1D fusion method [4] as described in the following is used.
Let us consider the following directional form of the within-group neutron transport equation:

$$\vec{\Omega}_n \cdot \nabla \psi^g(\vec{r},\vec{\Omega}_n) + \sigma^g(\vec{r})\,\psi^g(\vec{r},\vec{\Omega}_n) = q^g(\vec{r},\vec{\Omega}_n), \tag{1}$$

where standard notations are used.[6] For 3-D cartesian coordinates, we obtain the following equation by integrating Eq. (1) over z-direction interval ($z_{k-1/2}$, $z_{k+1/2}$):

$$\mu_n \frac{\partial \psi^g_{n,k}(x,y)}{\partial x} + \eta_n \frac{\partial \psi^g_{n,k}(x,y)}{\partial y} + \frac{\xi_n}{\Delta_k}[\psi^g_{n,k+1/2}(x,y) - \psi^g_{n,k-1/2}(x,y)] + \sigma^g_k(x,y)\,\psi^g_{n,k}(x,y) = q^g_{n,k}(x,y), \tag{2a}$$

where

$$\psi^g_{n,k}(x,y) = \frac{1}{\Delta_k}\int_{z_{k-1/2}}^{z_{k+1/2}} dz\,\psi^g_n(x,y,z), \tag{2b}$$

$$\psi^g_{n,k\pm1/2}(x,y) = \psi^g_n(x,y,z_{k\pm1/2}), \quad \Delta_k = z_{k+1/2} - z_{k-1/2}, \tag{2c}$$

$$q^g_{n,k}(x,y) = \sum_{g'=1}^{G}\sum_{l=0}^{L}\sum_{m=-l}^{l} Y_{lm}(\overrightarrow{\Omega_n})\,\sigma^{g'\to g}_{sl,k}(x,y)\sum_{n'} w_{n'} Y^*_{lm}(\overrightarrow{\Omega_{n'}})\,\psi^{g'}_{n',k}(x,y) + \frac{\chi^g}{k_{eff}}\sum_{g'=1}^{G}\nu\sigma^{g'}_{f,k}(x,y)\sum_{n'} w_{n'}\psi^{g'}_{n',k}(x,y). \tag{2d}$$

$$\sigma_k^g(x,y)=\frac{1}{\psi_{n,k}^g(x,y)\Delta_k}\int_{z_{k-1/2}}^{z_{k+1/2}}dz\,\sigma^g(x,y,z)\psi_n^g(x,y,z). \tag{2e}$$

Note that we consider in this study piece-wise homogeneous properties in axial direction cell by cell.

Rewriting Eq. (2a), the equation can be given in two-dimensional form as

$$\mu_n\frac{\partial\psi_{n,k}^g}{\partial x}+\eta_n\frac{\partial\psi_{n,k}^g}{\partial y}+\sigma_k^g(x,y)\,\psi_{n,k}^g(x,y)=Q_{n,k}^g(x,y), \tag{3a}$$

where

$$Q_{n,k}^g(x,y)=q_{n,k}^g(x,y)-\frac{\xi_n}{\Delta_k}[\psi_{n,k+1/2}^g(x,y)-\psi_{n,k-1/2}^g(x,y)]. \tag{3b}$$

Eq. (3a) is solved by the method of characteristics using the existing CRX code system with heterogeneous geometry maintained. But the source term is modified by the z-directional angular fluxes in Eq. (3b) at cell axial interfaces.

Now a 1-D axial equation is derived to update this modifying source term in Eq. (3b). To evaluate the z-directional outgoing angular fluxes,"online cell-wise homogenization" is considered. Integrating Eq. (1) over x-y domain ($x_{i-1/2}$, $x_{i+1/2}$) and ($y_{j-1/2}$, $y_{j+1/2}$) of cell (i,j), we obtain

$$\frac{\mu_n}{\Delta_i}[\psi_{n,i+1/2,j}^g(z)-\psi_{n,i-1/2,j}^g(z)]+\frac{\eta_n}{\Delta_j}[\psi_{n,i,j+1/2}^g(z)-\psi_{n,i,j-1/2}^g(z)]$$
$$+\xi_n\frac{d\psi_{n,i,j}^g(z)}{dz}+\sigma_{n,i,j}^g(z)\,\psi_{n,i,j}^g(z)=q_{n,i,j}^g(z), \tag{4a}$$

where

$$\psi_{n,i\pm1/2,j}^g(z)=\frac{1}{\Delta_j}\int_{y_{j-1/2}}^{y_{j+1/2}}dy\,\psi_n^g(x_{i\pm1/2},y,z), \tag{4b}$$

$$\psi_{n,i,j\pm1/2}^g(z)=\frac{1}{\Delta_i}\int_{x_{i-1/2}}^{x_{i+1/2}}dx\,\psi_n^g(x,y_{j\pm1/2},z), \tag{4c}$$

$$\psi_{n,i,j}^g(z)=\frac{1}{\Delta_i}\int_{x_{i-1/2}}^{x_{i+1/2}}dx\frac{1}{\Delta_j}\int_{y_{j-1/2}}^{y_{j+1/2}}dy\,\psi_n^g(x,y,z), \tag{4d}$$

$$\sigma_{n,i,j}^g(z)=\frac{1}{\psi_{n,i,j}^g(z)}\frac{1}{\Delta_i}\int_{x_{i-1/2}}^{x_{i+1/2}}dx\frac{1}{\Delta_j}\int_{y_{j-1/2}}^{y_{j+1/2}}dy\sigma^g(x,y,z)\psi_n^g(x,y,z). \tag{4e}$$

Rewriting Eq. (4a), we obtain then

$$\xi_n\frac{d\psi_{n,i,j}^g(z)}{dz}+\sigma_{n,i,j}^g(z)\,\psi_{n,i,j}^g(z)=Q_{n,i,j}^g(z), \tag{5a}$$

where

$$Q^g_{n,i,j}(z) = q^g_{n,i,j}(z) - \frac{\mu_n}{\Delta_i}[\psi^g_{n,i+1/2,j}(z) - \psi^g_{n,i-1/2,j}(z)] - \frac{\eta_n}{\Delta_j}[\psi^g_{n,i,j+1/2}(z) - \psi^g_{n,i,j-1/2}(z)]. \quad (5b)$$

To solve Eq. (5a), we integrate Eq. (5a) over z-directional interval ($z_{k-1/2}$, $z_{k+1/2}$) of cell (*i*,*j*,*k*) resulting in a balance equation,

$$\frac{\xi_n}{\Delta_k}(\psi^g_{n,i,j,k+1/2} - \psi^g_{n,i,j,k-1/2}) + \sigma^g_{n,i,j,k}\,\psi^g_{n,i,j,k} = Q^g_{n,i,j,k}, \quad (6a)$$

where

$$\psi^g_{n,i,j,k\pm1/2} = \psi^g_{n,i,j}(z_{k\pm1/2}), \quad (6b)$$

$$\psi^g_{n,i,j,k} = \frac{1}{\Delta_k}\int_{z_{k-1/2}}^{z_{k+1/2}} dz\,\psi^g_{n,i,j}(z), \quad (6c)$$

$$\sigma^g_{n,i,j,k} = \frac{1}{\psi^g_{n,i,j,k}}\frac{1}{\Delta_k}\int_{z_{k-1/2}}^{z_{k+1/2}} dz\,\sigma^g_{n,i,j}(z)\,\psi^g_{n,i,j}(z), \quad (6d)$$

$$= \frac{1}{\psi^g_{n,i,j,k}}\frac{1}{\Delta_i\Delta_j\Delta_k}\int_{z_{k-1/2}}^{z_{k+1/2}} dz\int_{x_{i-1/2}}^{x_{i+1/2}} dx\int_{y_{j-1/2}}^{y_{j+1/2}} dy\,\sigma^g(x,y,z)\,\psi^g_n(x,y,z). \quad (6e)$$

Since we consider piecewise homogeneous properties in axial direction, Eq. (6e) can be represented as

$$\sigma^g_{n,i,j,k} = \frac{\sum_{m\in cell(i,j,k)} \sigma^g_k(m)\,\psi^g_{n,k}(m)\,A_m}{\sum_{m\in cell(i,j,k)} \psi^g_{n,k}(m)\,A_m}, \quad (7)$$

where A_m is the area of radial computational mesh m and the average angular fluxes are obtained from the results of 2D MOC calculation. Eq. (6a) can be solved conveniently by various S_N-like methods using various auxiliary equations, e.g., diamond difference (DD), linear discontinuous (LD), quadratic discontinuous (QD), or linear multiple balance (LMB) scheme. A simple choice is the DD scheme:

$$\psi^g_{n,i,j,k} = \frac{1}{2}(\psi^g_{n,i,j,k+1/2} + \psi^g_{n,i,j,k-1/2}). \quad (8)$$

These z-directional angular surface fluxes are then used to update the modifying source term in Eq. (3b). Prior to this, the z-directional angular surface-averaged fluxes can be "modulated" to improve the cell-wise homogenization. The CMR method is used for acceleration on inner and outer iterations as in 2-D calculation.

4. NUMERICAL TESTS AND RESULTS

Table 1 shows the results for the 2-D standard calculation. The multiplication factor is 1.18813 and the maximum/minimum pin powers are 2.498/0.233. The reference eigenvalue provided by OECD[7] is 1.18655. Fig. 1a depicts trend of the eigenvalues as a function of the number of computational meshes. There is no significant difference as the number of computational meshes increases. Fig. 1b shows that the eigenvalues are sensitive to the number of azimuthal angles if it is less than 8. Figure 2 shows positions which have maximum/minimum pin power and maximum discrepancy.

The 2D/1D fusion method in the CRX code was applied to the seven-group three-dimensional OECD benchmark problem (C5G7MOX) which contains a MOX fuel assembly.[5] In this paper, the results of two cases for the 3-D C5G7 MOX benchmark problem are reported. In each case, we used 8 azimuthal/ 2 polar angles per octant, 50 rays per cell and direction. In a coarse case, 24 computational meshes per cell, and 6 axial nodes (2 for reflector region and 4 for fuel region) were used. In a fine case, 40 computational meshes per cell, and 10 axial nodes (1 for reflector region and 9 for fuel region) were used. The multiplication factor and the maximum/minimum pin powers are shown in Table 1. The reference values[8] are also shown in Table 1. Figure 3 shows positions which have maximum/minimum pin power and maximum discrepancy. Their detail distributions in each assembly are given in Figs. 4 through 6. Fig. 7 depicts error behaviors of fission source and multiplication factor with and without CMR acceleration. The CMR acceleration provides significant improvement in convergence than the source iteration (SI), and it took 42 outer iterations for this problem.

5. CONCLUSIONS

The CRX code based on the method of characteristics has performed 2-D calculation of the C5G7 MOX benchmark problem and it has been successfully extended to 3-D calculation with a fusion technique. This new approach reduces the huge memory and computing time problem of the direct extension of MOC to three-dimensional calculation. In addition, the S_N-like axial calculation takes advantage of the simpler axial structure of the core. The results indicate that the CRX code provides very accurate solutions in comparison with the reference solutions.

REFERENCES

[1] S.G. Hong and N.Z. Cho, "CRX: A Code for Rectangular and Hexagonal Lattices Based on the Method of Characteristics," *Ann. Nucl. Energy*, **25**, 547 (1998).

[2] G.S. Lee, N.Z. Cho, and S.G. Hong, "Acceleration and Parallelization of the Method of Characteristics for Lattice and Whole-Core Heterogeneous Calculations," *Proc. PHYSOR 2000,* Session II-C, Pittsburgh, USA, May 7-11, 2000.

[3] N.Z. Cho, *et. al.,*"Whole-Core Heterogeneous Transport Calculations and Their Comparison with Diffusion Results," *Trans. Am. Nucl. Soc.,* **83**, 292 (2000).

[4] N.Z. Cho, *et. al.,*"Fusion of Method of Characteristics and Nodal Method for 3-D Whole-Core Transport Calculation," *Trans. Am. Nucl. Soc.,* **86**, 322 (2002).

[5] E.E. Lewis, *et. al., Expert Group on 3-D Radiation Transport Benchmarks Summary of Meeting on C5G7MOX Benchmark,* NEA/NSC/DOC(2001)17, 2001.

[6] E.E. Lewis and W.F. Miller, Jr., *Computational Methods of Neutron Transport*, John Wiley & Sons, 1984.

[7] Excel format file provided by OECD, *2D-C5G7MOX-Ref-Solution-Smith.xls*, April 2002.

[8] Excel format file provided by OECD, *3D-C5G7MOX-Ref-Solution-Smith(1).xls*, May 2002.

Table 1. Summary of 2-D and 3-D results

		k_{eff}	k_{eff} discrepancy	Max/Min Power
2-D	CRX	1.18813	0.13%	2.498/0.233
	Reference	1.18655	-	2.498/0.232
3-D	CRX (coarse[a])	1.18528	0.12%	2.497/0.233
	CRX (fine[b])	1.18536	0.13%	2.496/0.233
	Reference	1.18381	-	2.500/0.231

[a] 24 meshes/cell, 6 axial nodes (4 nodes in fuel region, 2 nodes in reflector region)

[b] 40 meshes/cell, 10 axial nodes (9 nodes in fuel region, 1 node in reflector region)

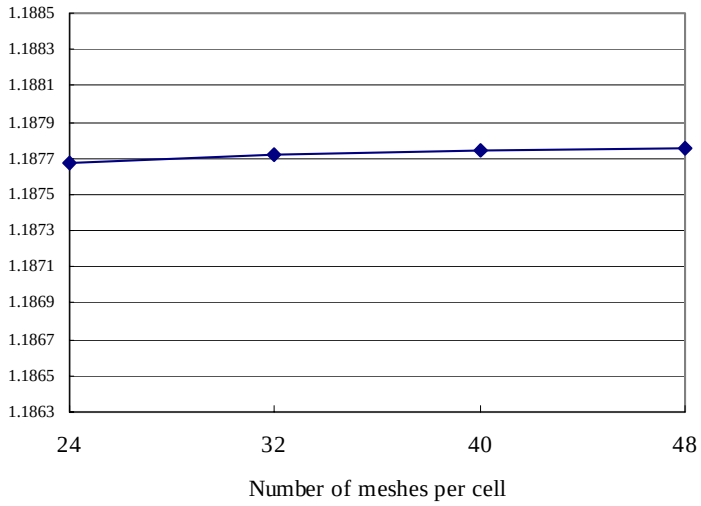

Fig. 1a. Eigenvalues versus computational meshes per cell in 2-D calculation.

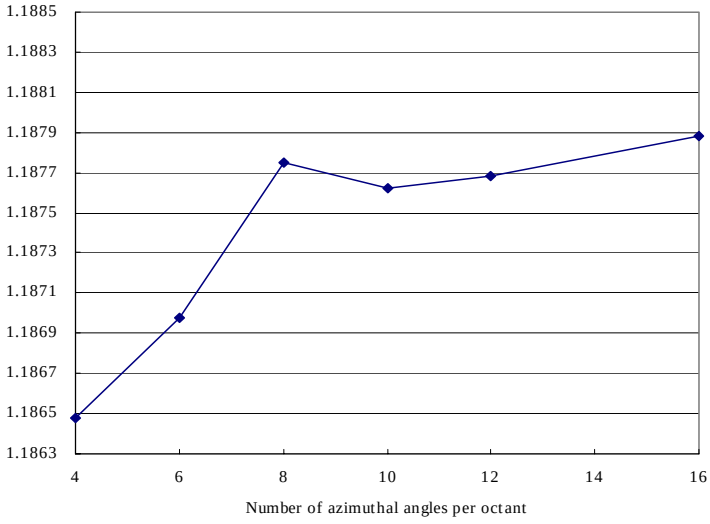

Fig. 1b. Eigenvalues versus azimuthal angles per octant in 2-D calculation.

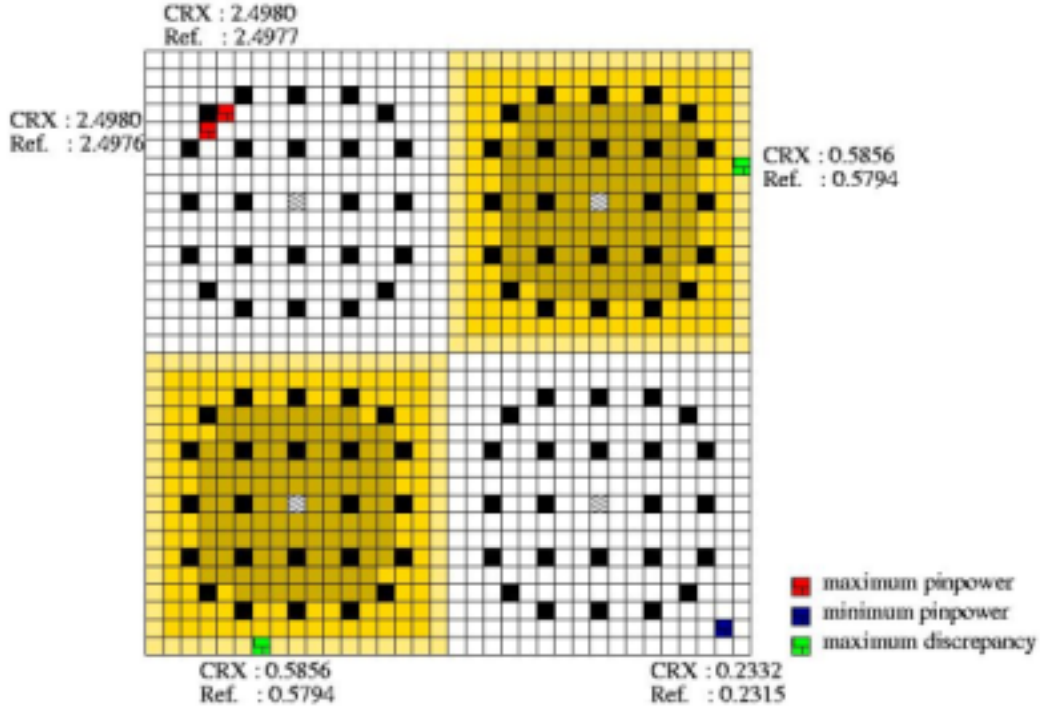

Fig. 2. Min/max pin power positions from 2-D results.

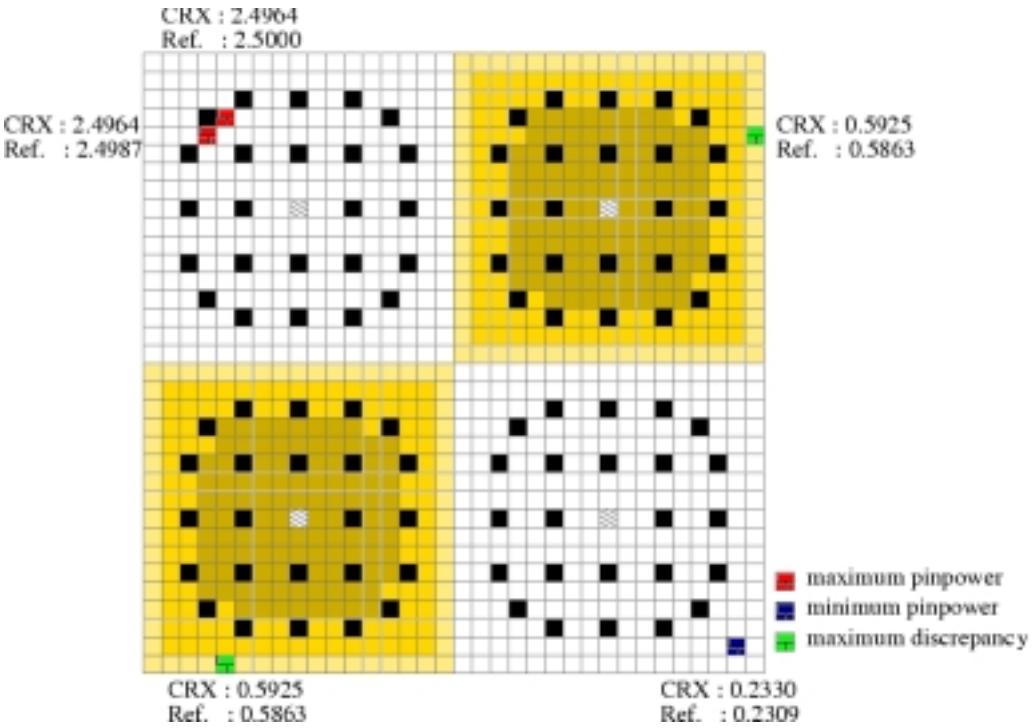

Fig. 3. Min/max pin power positions from 3-D results.

2.198	2.203	2.213	2.225	2.229	2.230	2.186	2.149	2.120	2.056	2.000	1.948	1.855	1.753	1.631	1.483	1.279
2.203	2.215	2.240	2.276	2.305	2.369	2.256	2.215	2.247	2.120	2.062	2.070	1.920	1.795	1.653	1.491	1.279
2.213	2.240	2.314	2.440	2.469		2.380	2.332		2.233	2.174		2.058	1.927	1.711	1.510	1.284
2.225	2.276	2.440		2.496	2.452	2.297	2.247	2.288	2.151	2.100	2.141	2.077		1.809	1.538	1.291
2.229	2.305	2.469	2.496	2.405	2.425	2.281	2.234	2.275	2.139	2.086	2.118	2.003	1.970	1.829	1.561	1.296
2.230	2.369		2.452	2.425		2.345	2.298		2.202	2.144		2.023	1.936		1.609	1.299
2.186	2.256	2.380	2.297	2.281	2.345	2.220	2.180	2.222	2.088	2.033	2.053	1.905	1.816	1.764	1.531	1.275
2.149	2.215	2.332	2.247	2.234	2.298	2.180	2.141	2.183	2.052	1.997	2.015	1.868	1.779	1.732	1.506	1.256
2.120	2.247		2.288	2.275		2.222	2.183		2.094	2.037		1.907	1.814		1.535	1.244
2.056	2.120	2.233	2.151	2.139	2.202	2.088	2.052	2.094	1.969	1.917	1.936	1.795	1.711	1.668	1.451	1.211
2.000	2.062	2.174	2.100	2.086	2.144	2.033	1.997	2.037	1.917	1.868	1.888	1.754	1.675	1.630	1.418	1.184
1.948	2.070		2.141	2.118		2.053	2.015		1.936	1.888		1.787	1.714		1.434	1.162
1.855	1.920	2.058	2.077	2.003	2.023	1.905	1.868	1.907	1.795	1.754	1.787	1.693	1.671	1.560	1.337	1.115
1.753	1.795	1.927		1.970	1.936	1.816	1.779	1.814	1.711	1.675	1.714	1.671		1.473	1.260	1.066
1.631	1.653	1.711	1.809	1.829		1.764	1.732		1.668	1.630		1.560	1.473	1.317	1.174	1.011
1.482	1.491	1.510	1.538	1.561	1.609	1.531	1.506	1.535	1.451	1.418	1.434	1.337	1.260	1.174	1.079	0.952
1.279	1.279	1.284	1.291	1.296	1.299	1.275	1.256	1.244	1.211	1.184	1.162	1.115	1.066	1.011	0.952	0.877

0.01	0.06	0.11	-0.00	0.14	-0.16	0.01	0.18	-0.09	0.07	0.08	-0.05	0.09	-0.08	0.02	0.04	-0.17
0.01	0.09	-0.11	-0.15	-0.13		-0.21	-0.24		-0.05	-0.03		0.07	-0.25	0.05	-0.05	-0.22
0.07	0.05	-0.13		-0.14	-0.14	0.08	0.01	-0.22	0.17	0.16	-0.09	-0.13		-0.30	-0.05	-0.11
0.01	0.24	-0.08	-0.09	0.00	-0.07	0.07	0.06	-0.16	0.07	0.17	-0.11	0.21	-0.18	-0.16	-0.09	-0.13
0.06	-0.05		-0.06	-0.10		-0.15	-0.22		0.06	-0.05		-0.11	-0.14		-0.28	-0.31
0.19	0.12	-0.08	0.29	0.18	-0.08	0.07	0.12	-0.05	0.06	0.02	-0.16	0.16	0.13	-0.29	-0.06	-0.03
0.14	0.01	-0.15	0.09	0.08	-0.28	0.07	0.02	-0.18	0.07	0.16	-0.17	0.10	-0.06	-0.27	-0.02	-0.19
0.07	-0.10		-0.21	-0.18		-0.19	-0.18		-0.01	-0.03		-0.07	-0.17		-0.14	-0.20
0.04	0.26	-0.20	0.04	0.06	-0.12	0.19	0.13	-0.11	0.22	0.13	-0.20	0.01	-0.20	-0.28	-0.20	-0.13
0.10	0.04	-0.15	0.11	0.08	-0.16	0.14	-0.11	-0.13	0.08	0.18	-0.19	0.10	0.05	-0.29	-0.12	-0.22
0.04	0.05		-0.19	-0.13		0.07	-0.11		-0.11	-0.19		-0.10	-0.24		-0.25	-0.22
-0.01	0.19	-0.09	-0.23	0.13	0.01	0.07	0.18	-0.18	-0.00	-0.02	0.05	0.08	-0.10	-0.27	0.04	-0.13
0.09	-0.05	-0.10	0.00	-0.29	-0.15	0.09	0.06	-0.20	0.21	-0.05	-0.15	-0.05		-0.36	-0.10	0.07
-0.04	-0.01	-0.11	-0.23	-0.17		-0.27	-0.25		-0.17	-0.19		-0.09	-0.22	-0.32	0.07	0.07
0.11	-0.10	-0.10	0.04	0.07	-0.15	-0.01	0.07	-0.08	-0.12	0.06	-0.24	-0.05	-0.22	-0.22	-0.20	-0.32
0.14	-0.14	-0.04	0.06	0.02	-0.05	-0.23	0.04	-0.13	-0.05	-0.14	-0.31	-0.14	0.00	-0.18	-0.39	-0.25

Fig. 4. Pin power and its relative percent discrepancy to reference value distributions of inside UO2 assembly from 3-D results with 10 axial nodes. (maximum power at shaded pin)

1.314	1.063	0.937	0.864	0.812	0.768	0.713	0.664	0.621	0.570	0.525	0.484	0.438	0.399	0.378	0.412	0.605
1.297	1.346	1.173	1.095	1.050	1.044	0.921	0.852	0.838	0.735	0.674	0.657	0.568	0.505	0.472	0.520	0.597
1.291	1.324	1.180	1.174	1.118		0.949	0.869		0.755	0.688		0.606	0.542	0.477	0.511	0.593
1.293	1.336	1.262		1.111	1.127	0.960	0.883	0.876	0.761	0.700	0.702	0.589		0.513	0.517	0.592
1.296	1.363	1.288	1.181	1.147	1.083	0.931	0.857	0.852	0.740	0.679	0.677	0.612	0.538	0.518	0.527	0.592
1.297	1.425		1.279	1.142		0.983	0.901		0.784	0.713		0.620	0.577		0.552	0.592
1.275	1.336	1.222	1.150	1.040	1.036	0.902	0.834	0.832	0.721	0.661	0.653	0.563	0.523	0.488	0.518	0.586
1.257	1.315	1.198	1.126	1.020	1.016	0.889	0.823	0.821	0.713	0.653	0.643	0.554	0.514	0.480	0.512	0.580
1.244	1.362		1.188	1.073		0.942	0.867		0.757	0.688		0.589	0.541		0.534	0.577
1.213	1.272	1.162	1.092	0.991	0.990	0.865	0.802	0.802	0.695	0.638	0.629	0.542	0.503	0.471	0.501	0.568
1.187	1.247	1.141	1.077	0.977	0.974	0.851	0.790	0.788	0.685	0.629	0.621	0.536	0.500	0.467	0.496	0.561
1.165	1.286		1.161	1.042		0.904	0.831		0.728	0.664		0.578	0.539		0.518	0.556
1.122	1.190	1.134	1.041	1.017	0.968	0.834	0.772	0.772	0.671	0.619	0.619	0.560	0.493	0.477	0.486	0.546
1.078	1.128	1.078		0.962	0.981	0.841	0.778	0.775	0.677	0.626	0.630	0.530		0.465	0.468	0.536
1.036	1.086	0.987	0.996	0.958		0.823	0.760		0.668	0.612		0.544	0.488	0.430	0.461	0.532
1.007	1.093	0.987	0.943	0.918	0.922	0.821	0.767	0.759	0.671	0.619	0.606	0.528	0.472	0.441	0.481	0.540
1.013	0.910	0.855	0.819	0.787	0.756	0.711	0.669	0.631	0.585	0.542	0.503	0.459	0.420	0.398	0.423	0.580

0.10	0.03	0.08	-0.11	-0.25	-0.10	-0.06	-0.33	-0.33	-0.25	-0.18	-0.21	-0.49	-0.33	0.02	0.34	0.80
0.13	0.26	0.27	0.23	-0.04	-0.31	0.04	0.28	-0.27	0.10	0.15	-0.51	-0.00	0.11	0.41	0.69	0.76
0.07	0.39	0.13	-0.22	-0.24		-0.07	-0.20		-0.32	-0.21		-0.43	-0.01	0.34	0.42	0.74
0.04	0.23	0.05		-0.10	-0.08	0.10	0.19	-0.10	0.42	0.38	0.01	0.22		-0.15	0.76	0.97
0.08	0.47	-0.00	-0.05	0.11	-0.35	0.18	0.27	-0.05	0.26	0.36	0.21	-0.02	0.09	0.09	0.95	1.05
0.15	-0.19		-0.22	-0.15		-0.28	-0.34		0.02	-0.24		-0.03	-0.01		0.52	0.85
0.13	0.25	-0.26	0.02	0.33	-0.06	0.14	-0.04	-0.14	0.21	0.25	0.02	0.12	0.58	0.32	0.76	0.48
0.06	0.26	-0.19	0.25	0.02	-0.32	0.10	0.24	0.21	0.11	0.20	-0.10	0.08	0.36	-0.20	0.87	0.85
0.05	-0.31		-0.33	0.01		-0.23	-0.28		-0.06	-0.30		-0.12	-0.12		0.40	0.75
-0.09	0.01	-0.00	0.40	0.21	-0.22	0.04	-0.21	-0.24	0.06	0.04	-0.23	-0.13	0.32	0.24	0.45	0.71
0.16	0.38	-0.13	0.33	0.09	-0.34	0.32	0.48	-0.18	0.36	0.24	-0.30	0.11	0.38	-0.06	0.13	0.78
0.17	-0.08		-0.07	-0.26		-0.24	-0.24		-0.20	-0.20		-0.24	0.15		0.32	0.43
0.03	0.26	-0.19	-0.05	0.35	-0.08	0.20	-0.04	-0.29	0.13	-0.02	-0.07	0.32	0.03	0.22	0.71	0.71
0.01	0.11	-0.21		-0.07	-0.20	0.29	0.26	0.06	-0.01	0.30	-0.23	-0.14		-0.08	0.61	1.01
0.17	0.24	0.11	-0.01	-0.12		-0.25	-0.13		-0.38	-0.23		-0.17	-0.25	0.11	0.48	0.78
-0.08	0.17	0.21	0.18	0.11	-0.08	0.32	0.18	-0.11	-0.02	-0.04	-0.31	0.34	0.19	0.20	0.82	0.53
-0.24	0.06	0.03	-0.14	0.02	0.14	0.15	0.09	0.12	-0.28	-0.36	-0.00	-0.00	0.05	0.48	0.43	0.84

Fig. 5. Pin power and its relative percent discrepancy to reference value distributions of MOX assembly from 3-D results with 10 axial nodes. (maximum discrepancy at shaded pin)

0.793	0.789	0.770	0.749	0.724	0.698	0.658	0.621	0.587	0.544	0.505	0.470	0.429	0.394	0.374	0.392	0.505
0.789	0.825	0.830	0.824	0.810	0.805	0.739	0.696	0.678	0.612	0.568	0.546	0.486	0.442	0.414	0.426	0.531
0.770	0.830	0.863	0.896	0.884		0.798	0.751		0.663	0.615		0.535	0.488	0.440	0.440	0.537
0.749	0.824	0.896		0.889	0.849	0.768	0.723	0.707	0.637	0.594	0.579	0.539		0.465	0.445	0.533
0.724	0.810	0.884	0.889	0.839	0.822	0.749	0.706	0.691	0.624	0.581	0.565	0.513	0.492	0.463	0.444	0.523
0.698	0.805		0.849	0.822		0.751	0.708		0.628	0.584		0.508	0.472		0.445	0.509
0.658	0.739	0.798	0.768	0.749	0.751	0.689	0.653	0.641	0.579	0.539	0.522	0.465	0.432	0.425	0.413	0.486
0.621	0.696	0.751	0.723	0.706	0.708	0.653	0.619	0.608	0.550	0.512	0.495	0.441	0.409	0.403	0.393	0.463
0.587	0.678		0.707	0.691		0.641	0.608		0.541	0.504		0.435	0.402		0.385	0.441
0.544	0.612	0.663	0.637	0.624	0.628	0.579	0.550	0.541	0.489	0.456	0.442	0.394	0.365	0.360	0.351	0.413
0.505	0.568	0.615	0.594	0.581	0.584	0.539	0.512	0.504	0.456	0.426	0.412	0.368	0.342	0.337	0.328	0.386
0.470	0.546		0.579	0.565		0.522	0.495		0.442	0.412		0.359	0.334		0.316	0.360
0.429	0.486	0.535	0.539	0.513	0.508	0.465	0.441	0.435	0.394	0.368	0.359	0.326	0.312	0.296	0.282	0.330
0.394	0.442	0.488		0.492	0.472	0.432	0.409	0.402	0.365	0.342	0.334	0.312		0.270	0.257	0.302
0.374	0.414	0.440	0.465	0.463		0.425	0.403		0.360	0.337		0.296	0.270	0.242	0.237	0.278
0.392	0.426	0.440	0.445	0.444	0.445	0.413	0.393	0.385	0.351	0.328	0.316	0.282	0.257	0.237	0.233	0.268
0.505	0.531	0.537	0.533	0.523	0.509	0.486	0.463	0.441	0.413	0.386	0.360	0.330	0.302	0.278	0.268	0.288

-0.43	-0.50	-0.48	-0.24	-0.02	-0.21	-0.34	-0.38	-0.32	-0.21	-0.25	-0.18	-0.37	-0.17	-0.05	0.23	0.18
-0.38	-0.30	-0.39	-0.25	-0.17	-0.52	-0.11	-0.11	-0.31	-0.23	-0.00	-0.59	-0.21	-0.20	0.03	0.18	0.26
-0.56	-0.25	-0.07	-0.48	-0.24		-0.44	-0.40		-0.11	-0.07		0.07	-0.33	0.17	0.53	0.55
-0.17	-0.38	-0.32		-0.24	-0.37	-0.04	0.18	-0.34	-0.05	-0.17	-0.28	-0.35		0.12	0.27	0.42
-0.06	-0.22	-0.34	-0.22	-0.11	-0.17	0.11	0.10	-0.25	-0.03	0.04	-0.09	0.11	-0.05	0.22	0.41	0.93
-0.05	-0.23		-0.38	-0.30		-0.24	-0.36		-0.09	-0.24		-0.42	-0.22		0.08	0.55
-0.14	-0.02	-0.11	0.21	0.06	-0.17	-0.01	0.22	0.02	0.18	-0.03	-0.17	0.03	-0.22	-0.14	0.37	0.63
-0.22	0.18	-0.09	-0.04	0.05	-0.20	0.09	0.27	-0.13	0.04	0.30	0.11	0.33	-0.06	0.13	0.35	0.63
-0.28	-0.15		-0.21	-0.30		-0.07	-0.07		0.13	-0.15		0.03	-0.15		0.14	0.68
-0.12	0.11	0.19	-0.16	-0.17	-0.38	0.03	0.16	0.01	0.32	-0.17	-0.24	0.26	0.08	-0.15	0.31	0.55
0.02	-0.43	-0.25	-0.24	-0.16	-0.49	0.12	0.14	-0.26	0.23	0.13	-0.44	-0.11	0.18	-0.11	0.21	0.52
-0.29	-0.42		-0.51	-0.44		-0.57	-0.29		-0.29	-0.41		-0.18	-0.47		-0.04	0.25
-0.19	-0.21	-0.19	-0.17	-0.10	-0.30	0.20	-0.31	-0.60	-0.36	0.01	-0.21	-0.01	-0.53	-0.28	0.15	0.51
-0.28	0.01	-0.19		-0.15	-0.26	-0.17	-0.28	-0.36	-0.01	0.17	-0.26	-0.12		-0.30	0.68	0.40
-0.30	0.11	-0.05	-0.03	-0.26		-0.47	-0.27		0.08	-0.11		-0.13	0.21	0.35	0.39	0.53
0.11	0.16	0.36	0.34	0.08	-0.09	0.10	0.41	0.20	0.35	0.55	-0.00	0.42	0.44	0.71	0.87	0.43
0.27	0.28	0.33	0.40	0.39	0.63	0.28	0.44	0.51	0.57	0.54	0.62	0.51	0.59	0.51	0.53	0.75

Fig. 6. Pin power and its relative percent discrepancy to reference value distributions of outside UO2 assembly from 3-D results with 10 axial nodes. (minimum power at shaded pin)

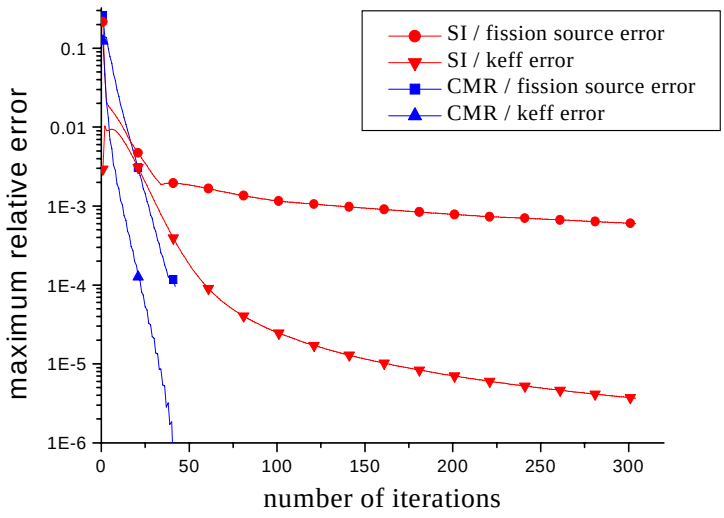

Fig. 7. Error behavior with/without CMR acceleration in 3D calculation with 6 axial nodes.